RSC Advances

ROYAL SOCIETY OF CHEMISTRY

www.rsc.org/advances

Isoindigo-Based Microporous Organic Polymers for Carbon Dioxide Capture

Yang Zhao, Xiaoyan Wang, Chong Zhang, Fangyuan Xie, Rui Kong, Jia-Xing Jiang*

Key Laboratory for Macromolecular Science of Shaanxi Province, School of Materials Science and Engineering, Shaanxi Normal University, Xi'an, Shaanxi, 710062, P. R. China.

E-mail: jiaxing@snnu.edu.cn

Abstract

Isoindigo-based microporous organic polymers from nitrogen- and oxygen-rich 6,6'-dibromoisoindigo and its alkylated derivatives have been synthesized via palladium-catalyzed Sonogashira-Hagihara cross-coupling reaction. The pore properties (pore size & surface area) of this kind of microporous organic polymers could be tuned by the alkyl groups connected with 6,6'-dibromoisoindigo unit. Owing to the incorporation of nitrogen atoms and ketonic groups from the isoindigo unit into the skeleton of the microporous polymers enhanced the binding affinity between the pore wall and CO_2 molecules, the polymers show high isosteric heats of CO_2 adsorption of 27.4~33.5 kJ mol^{-1}, which are higher than those of many reported porous organic polymers. Compared with the alkylated polymers of TBMIDM and TBMIDE, TBMID without alkyl group exhibits a high CO_2 uptake ability of 3.30 mmol g^{-1} (1.13 bar/273 K) with a CO_2/N_2 sorption selectivity of 58.8:1 because of the strong interactions between the polymer network and the polarizable CO_2 molecules through dipole−quadrupole interactions and/or hydrogen bonding. These data demonstrate that these isoindigo-based microporous organic polymers would be potential candidates for applications in post-combustion CO_2 capture and sequestration.

Keywords: microporous polymers, isoindigo, gas adsorption, isosteric heats

1. Introduction

Carbon dioxide is deemed as a significant contribution to global warming and some environment issues. Developing highly efficient carbon capture and separation technologies or CO_2 capture materials would be potential strategies to address these issues. The amine-based wet scrubbing technology for CO_2 capture suffers from the considerable energy penalty for CO_2 release and the regeneration of amine solution.[1] Porous solids, which adsorb CO_2 molecules through relative weak van der Waals force, are emerging as a new class of CO_2 capture materials. A range of porous solids have been proposed for capture of carbon dioxide, which mainly include microporous zeolites,[2] activated carbons,[3] metal organic frameworks (MOFs),[4] porous organic molecules,[5, 6] and microporous organic polymers (MOPs).[7, 8] Among of them, MOPs have attracted increasing recent attention because they show great potential in a variety of applications such as gas storage and separation,[9, 10] heterogeneous catalysis[11, 12] and chemical sensors.[13, 14] To date, a wide range of MOPs have been developed by using various building blocks and synthetic strategies. These mainly include polymers of intrinsic microporosity (PIMs),[15] covalent organic frameworks (COFs),[16, 17] conjugated microporous polymers (CMPs),[18-20] porous polymer networks (PPNs),[21] porous aromatic framework (PAFs),[22] covalent triazine-based frameworks (CTFs),[23] and hypercrosslinked porous polymers (HCPs).[24-26] However, most reported MOPs without polar group or heteroatom usually showed low CO_2 adsorption capacity at ambient temperatures and pressures because of the lack of strong CO_2 binding sites. Recent studies have revealed that the electron-rich porous polymers networks can yield strong dipole−quadrupole interaction with CO_2 molecules, leading to a significant increase in the CO_2 capture capacity, and thus a range of nitrogen-rich and/or oxygen-rich microporous organic polymers have been synthesized for

capturing CO_2. For example, the microporous polycarbazole of CPOP-1 with high nitrogen content showed a CO_2 capture capacity of 4.82 mmol g^{-1} and a CO_2/N_2 adsorption selectivity of 25 at 273 K/1.0 bar,[27] the imine-linked porous polymer framework of PPF-1 exhibited a CO_2 uptake of 6.1 mmol g^{-1} with a CO_2/N_2 adsorption selectivity of 14.5 at 273 K/1.0 bar,[28] the benzimidazole-linked polymer of BILP-4 could adsorb CO_2 up to 5.3 mmol g^{-1} with a CO_2/N_2 adsorption selectivity of 79 at 273 K/1.0 bar,[29] the nanoporous azo-linked polymer of ALP-1 showed a CO_2 uptake of 5.36 mmol g^{-1} with a CO_2/N_2 adsorption selectivity of 35 at 273 K/1.0 bar,[30] the porous triazine bifunctionalized task-specific polymer of TSP-2 could adsorb CO_2 up to 4.1 mmol g^{-1} with a CO_2/N_2 adsorption selectivity of 38 at 273 K/1.0 bar,[31] the nanoporous covalent organic polymer with tröger's base functionality of TB-COP-1 exhibited enhanced CO_2 capture capacity of 5.19 mmol g^{-1} with a CO_2/N_2 adsorption selectivity of 79.2 at 273 K,[32] the iron-containing porphyrin porous organic polymers showed a high CO_2 uptake ability of 4.30 mmol g^{-1} at 273 K/1.0 bar,[33] and the triazine-functionalized porphyrin-based porous organic polymer of TPOP-1 exhibited a CO_2 uptake as high as 6.2 mmol g^{-1} at 273 K/3.0 bar.[34] These results demonstrated that such electron-rich MOPs have great potential to increase the CO_2 uptake ability or CO_2/N_2 adsorption selectivity. Palladium-catalyzed Sonogashira–Hagihara cross-coupling polymerization has been widely used to produce a range of highly porous organic polymers. For example, the conjugated microporous poly(aryleneethynylene) networks synthesized by Sonogashira–Hagihara cross-coupling polymerization showed a high surface area up to 834 m^2 g^{-1}.[18] The CMPs with a range of chemical functionalities including carboxylic acids, amines, hydroxyl groups, and methyl groups exhibited high isosteric heat of sorption for CO_2.[35] The metal–organic conjugated microporous polymers produced by

Sonogashira–Hagihara coupling reaction could be used as heterogeneous catalyst.[36] The conjugated nanoporous polymer colloids were synthesized by using Sonogashira–Hagihara coupling reaction.[37] The cobalt/aluminium-coordinated CMPs exhibited outstanding CO_2 capture capacity and conversion performance at atmospheric pressure and room temperature.[38]

Isoindigo is an efficient acceptor species that has been studied widely in the areas of organic photovoltaic cells[39] and dye-sensitized solar cells.[40] However, to the best of our knowledge, there are no reports on the synthesis of porous polymers based on isoindigo or its derivatives. We present here the synthesis of a novel class of isoindigo-based MOPs via one-pot palladium-catalyzed Sonogashira–Hagihara cross-coupling reaction. Isoindigo contains both nitrogen and oxygen atoms, making the resulting porous polymer highly electron-rich, which could enhance the binding affinity between the adsorbent and CO_2 molecules, and thus we hypothesized that the introduction of isoindigo segments into the porous polymer skeleton could lead to the increase of CO_2 capture capacity. In addition, we also synthesized isoindigo-based MOPs with different alkyl substituents, and investigated the influence of alkyl substituent on the porosity and CO_2 capture capacity of the resulting porous polymers.

2. Experimental Section

Chemicals: 6-bromooxindole and 6-bromoisatin were purchased from TCI. Triphenylphosphine, tetraphenylmethane, trimethylsilylacetylene and Copper(I) iodide were purchased from Alfa. K_2CO_3 and bromoethane were purchased from Acros. Iodomethane, tetrakis(triphenylphosphine)palladium(0), bis(triphenylphosphine)palladium(II)chloride, N,N-dimethylformamide, triethylamine and other chemicals were purchased from J&K Scientific Ltd. All chemicals were used as received. 6,6'-dibromoisoindigo, 6,6'-dibromo-N,N'-(2-methyl)-isoindigo,

6,6'-dibromo-N,N'-(2-ethyl)-isoindigo[39] and tetra(4-ethynylphenyl)methane[41] were prepared according to the previously reported methods.

2.1 Synthesis of isoindigo-based microporous organic polymers

All of the polymer networks were synthesized by palladium(0)-catalyzed Sonogashira-Hagihara cross-coupling reacation of 6,6'-dibromoisoindigo, 6,6'-dibromo-N,N'-(2-methyl)-isoindigo or 6,6'-dibromo-N,N'-(2-ethyl)-isoindigo with tetra(4-ethynylphenyl)methane. All reactions were carried out at a fixed total molar monomer concentration of 75 mmol/L and a fixed reaction temperature and reaction time (100 ℃/48 h). A representative experimental procedure for TBMID is given as an example.

TBMID: 6,6'-dibromoisoindigo (206 mg, 0.5 mmol), tetra(4-ethynylphenyl)methane (107 mg, 0.25 mmol), tetrakis(triphenylphosphine)palladium(0) (15 mg), copper(I) iodide (10 mg) were dissolved in a mixture of DMF (5.0 mL) and Et_3N (5.0 mL). The mixture was degassed under freeze-pump-thaw, purged with N_2 and stirred at 100 ℃ for 48 h. The mixture was then cooled down to room temperature and the precipitated polymer network was filtered and washed with methanol, water, chloroform and acetone, respectively. Further purification of the polymer was carried out by Soxhlet extraction with methanol for 48 h. The product was dried in vacuum for 24 h at 70 ℃ and obtained as a dark red powder (209 mg, yield: 82%). Elemental combustion analysis (%) Calcd for $(C_{71}H_{44}N_4O_4)_n$: C 83.86, H 4.33, N 6.30; Found: C 75.09, H 4.26, N 4.83. The deviation of the elemental analysis from the theoretical value could be attributed to the unreacted end groups and the trapped gases and water from air in the porous polymers because of their high microporosities.[29]

2.2 Characterization

The FT-IR spectra were carried out in transmission on a Tensor 27 FT-IR spectrometer (Bruker) using KBr disks. The thermal properties of the polymer networks were evaluated using a thermogravimetric analysis (TGA) with a differential thermal analysis instrument (Q1000DSC + LNCS + FACS Q600SDT) over the temperature range from 30 to 800 ℃ under a nitrogen atmosphere with a heating rate of 10 ℃ min^{-1}. The morphology of the polymer networks were obtained on a field emission scanning electron microscope (SEM, JSM-6700F, JEOL, Japan) and a high resolution transmission electron microscopy (TEM, JEM-2100F, JEOL, Japan). Powder X-ray diffraction measurement was carried out on X-ray Deffractometer (D/Max-3c). Solid state magic angle spinning ^{13}C CP/MAS NMR measurement was carried out on a Bruker Avance III model 400 MHz NMR spectrometer at a MAS rate of 5 kHz. Elemental analysis was performed on a EURO EA3000 Elemental Analyzer. Surface areas and pore size distributions were measured by nitrogen adsorption and desorption at 77.3 K using an ASAP 2420-4 (Micromeritics) volumetric adsorption analyzer. The surface areas were calculated in the relative pressure (P/P_o) range from 0.05 to 0.20. Pore size distributions and pore volumes were derived from the N_2 adsorption branch of the isotherms using the non-local density functional theory (NL-DFT). Samples were degassed at 120 ℃ for 15 h under vacuum (10^{-5} bar) before analysis. Gas sorption isotherms were measured on an ASAP 2420-4 as well.

3. Results and Discussion

Scheme 1 shows the general synthetic route for the three isoindigo-based microporous organic polymers. 6,6'-Dibromoisoindigo and its alkylated derivatives with methyl or ethyl groups were employed as the building blocks in order to study the influence of alkyl groups on the pore properties and gas adsorption performances of the resulting polymers. Tetra(4-ethynylphenyl)methane was selected as the

comonomer since it possesses four reactive sites, which makes the polymers highly crosslinked molecular structures. All of the polymer networks were insoluble in common organic solvents such as THF, DMF, $CHCl_3$ and methanol. The resulting polymer networks showed high thermal stability in nitrogen atmosphere, as revealed by TGA (up to 350 ℃, Figure S1), and were also chemically stable. The FT-IR spectra of the polymer networks (Figure S2) structure show the aromatic C=C vibration bands at 1600 cm^{-1}, the alkyne of –C≡C– band at 2200 cm^{-1}, the stretching vibration band of C-N-C at 1494 cm^{-1}, and the C=O stretching vibrations at around 1705 cm^{-1} in all the samples. In addition, TBMID without any alkyl substituent showed the N-H stretching vibration at around 3213 cm^{-1} and the bending vibration at 1312 cm^{-1}, which were not observed for TBMIDM with methyl group and TBMIDE with ethyl group. The $–CH_3$ stretching vibration at around 2925 cm^{-1} and the bending vibration 1375 cm^{-1} could be detected for TBMIDM with methyl group. The $–CH_2–$, $–CH_3$ stretching vibration at around 2930 cm^{-1}, 2973 cm^{-1} and the bending vibration 1347 cm^{-1}, 1371 cm^{-1} could be respectively detected for TBMIDE with ethyl group. The polymer networks were also characterized at the molecular level by solid state $^{1}H–^{13}C$ cross-polarization magic-angle spinning (CP/MAS) NMR spectroscopy to further confirm the structure of the polymer networks. The $^{1}H–^{13}C$ CP/MAS NMR spectra and the assignment of the resonances are shown in Fig. 1. All of the polymer networks showed the characteristic peaks at approximately 169 ppm (–C=O), 144 ppm ($N-C_{ar}$), 110 ppm (–C=C–), 92 ppm (–C≡C–) and 65 ppm corresponding to the quaternary carbon atom that is connected to four phenyl groups. In addition, the signal at approximately 26 ppm from $–CH_3$ was observed for TBMIDM with methyl group, and the signals at approximately 35 ppm ($–CH_2–$) and 12 ppm ($–CH_3$) were also observed for TBMIDE with ethyl group, while these peaks were not observed in the

$^{1}H–^{13}C$ CP/MAS NMR spectrum of TBMID without any substitution. These results are consistent with the expected polymer networks. No any clear diffraction peaks could be observed in the powder X-ray diffraction profiles (Figure S3), indicating that the polymer networks are amorphous in nature. Scanning electron microscopy images reveled that the three polymers possess very similar morphology with relatively uniform solid submicrometer spheres (Figure S4), indicating that the alkyl group has negligible influence on the morphology of the resulting polymers. High resolution transmission electron microscopy (HR-TEM) images also demonstrated the amorphous structure of the polymer networks and the presence of homogenous pores in the polymers (Figure S5).

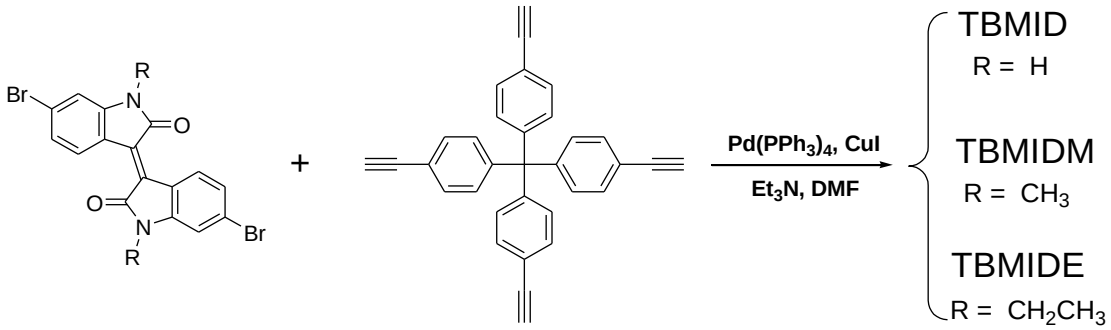

Scheme 1. Synthetic route to the isoindigo-based microporous organic polymers

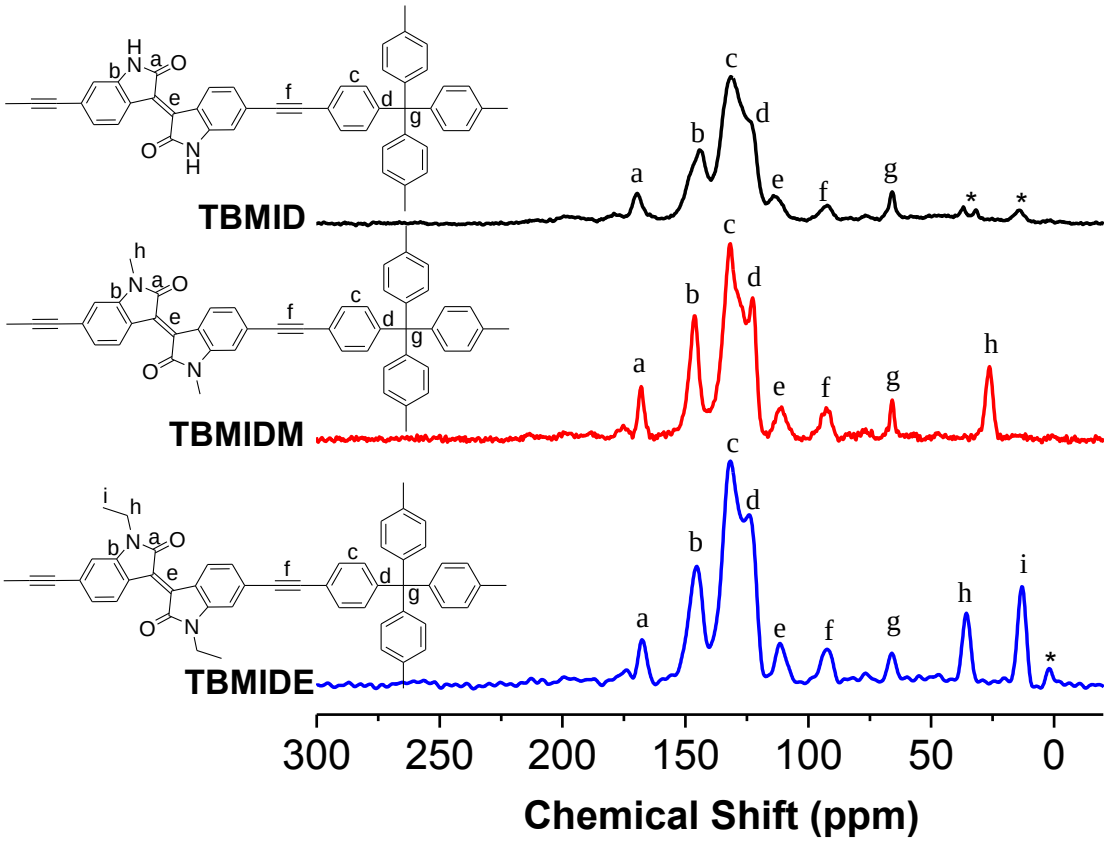

Figure 1. Solid-state $^{1}H–^{13}C$ CP-MAS NMR spectra of the polymer networks, asterisks denote spinning side bands.

The porosity of the polymer networks was measured by nitrogen adsorption and desorption analyses at 77.3 K. As shown in Fig. 2a, all of the resulting polymer networks gave rise to typically Type–I nitrogen gas sorption isotherms according to IUPAC classifications,[42] indicating that these polymer networks are microporous in nature. This was also evidenced by the pore size distribution (PSD) curves for the polymer networks as calculated using nonlocal density functional theory (NL-DFT). All of the polymer networks exhibited abundant micropore structure with pore size less than 2.0 nm (Figure 2b). Compared with TBMIDM and TBMIDE, TBMID without any substitution exhibited smaller micropore size centered at around 0.9 nm. TBMIDM showed a micropore size centered at around 1.1 nm and TBMIDE exhibited a micropore size centered at 1.0 nm, indicating that the pore size of the

polymer networks could be controlled by the substituent group, as observed in other reported CMPs with alkyl substituent.[43] Unlike the crystalline MOFs and COFs, where the pore size could be fine narrowed by increasing the substituent group grafted on the ligand or the building block,[44-46] these amorphous polymers do not show a simple and rational pore size order with increasing the substituent group from H to CH_3 to CH_2CH_3. For example, TBMID without alkyl group shows the smallest pore size of 0.9 nm, while TBMIDM with methyl group shows the biggest pore size of 1.1 nm as shown in Figure 2b. We do not at present have a full explanation for this result, but it could be partially attributed to the increased distance among the polymer chains because of the increasing steric hindrance from H to CH_3 to CH_2CH_3, which hinders the polymer to pack into small pores during the polymerization, similar result was observed for the other reported CMPs with different alkyl chains.[47] The apparent Brunauer-Emmet-Teller (BET) specific surface areas were found to be 688, 763 and 654 m^2 g^{-1} for TBMID, TBMIDM and TBMIDE, respectively. All the polymer networks showed high micropore surface area ratio over 90% and micropore volume ratio over 82% (Table 1), again suggesting that the pores of the polymer networks are dominated by micropores, which is in agreement with the shape of the nitrogen sorption isotherms.

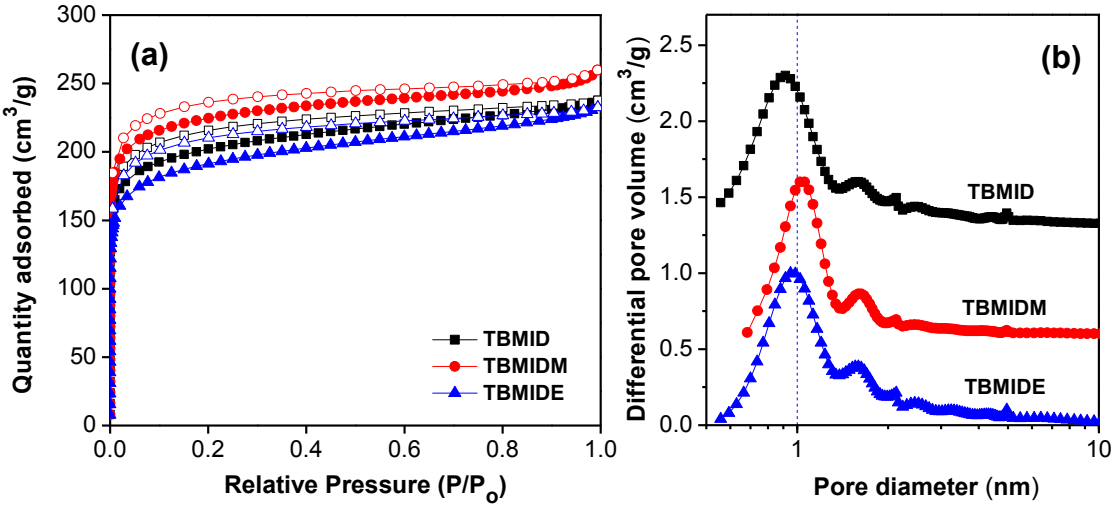

Figure 2. a) Nitrogen adsorption (filled symbols)/desorption (empty symbols) isotherms for the polymer networks collected at 77.3 K; b) Pore size distribution curves calculated by NL-DFT.

Table 1. Summary of pore properties for the polymer networks

Polymer	S_{BET} [a] [m^2 g^{-1}]	S_{Micro} [b] [m^2 g^{-1}]	V_{Micro} [c] [cm^3 g^{-1}]	V_{Total} [d] [cm^3 g^{-1}]	S_{Micro}/ S_{BET} [%]	V_{Micro}/ V_{Total} [%]
TBMID	688	629	0.30	0.35	91.4	85.7
TBMIDM	763	720	0.34	0.38	94.5	89.5
TBMIDE	654	588	0.28	0.34	89.9	82.4

[a] Surface area calculated from N_2 adsorption isotherm in the relative pressure (*P/Po*) range from 0.05 to 0.20; [b] Micropore surface area calculated from the N_2 adsorption isotherm using *t-plot* method based on the Harkins Jura Equation. [c] The micropore volume derived from the *t-plot* method; [d] Total pore volume at P/P_o = 0.90.

The microporous nature of these isoindigo functionalized polymer networks inspired us to investigate their gas uptake capacities. Figure 3a shows the hydrogen sorption curves of the three polymer networks measured at 77.3 K up to a pressure of 1.13 bar. TBMID without any alkyl substituent exhibited the largest hydrogen uptake capacity of 137 cm^3 g^{-1} (~1.23 wt%) among the three polymer networks, although it showed the lower surface area of 688 m^2 g^{-1} than that of TBMIDM (763 m^2 g^{-1}), which might be attributed to the narrower micropore size in TBMID enhanced the interaction between the pore wall and H_2 molecules.[48] The hydrogen uptake of

TBMID is comparable to that of some other porous polymers with much higher surface area at the same conditions, such as the dihydroxyl-functionalized conjugated microporous polymer of network-13 (1.14 wt%, S_{BET} = 853 m^2 g^{-1}),[49] the benzene-based CMP of CMP-0 (1.4 wt%, S_{BET} = 1018 m^2 g^{-1})[50] and the nanoporous organic framework of NPOF-2 (1.45 wt%, S_{BET} = 3127 m^2 g^{-1}),[51] although it is still lower than that of the carbazole-based CMP with the hydrogen uptake capacity of 2.80 wt% at 1.13 bar/77.3 K.[27]

The CO_2 uptakes of the polymer networks were measured up to 1.13 bar at 273 and 298 K, respectively (Figure 3b & 3c). It was found that TBMID showed a high CO_2 uptake ability of 3.30 mmol g^{-1} at 1.13 bar/273 K, which is higher than that of TBMIDM (2.56 mmol g^{-1}) with methyl group and TBMIDE (2.46 mmol g^{-1}) with ethyl group. The high CO_2 uptake ability of TBMID could be attributed to the strong interactions between the polymer network and the polarizable CO_2 molecules through dipole−quadrupole interactions and/or hydrogen bonding that utilize the protonated and proton-free nitrogen sites of isoindigo segments,[29] and the hydrogen bonding from the N-H of isoindigo segments might play a crucial role for increasing the CO_2 uptake ability, since TBMIDM and TBMIDE showed much lower CO_2 uptake ability compared with TBMID, which could be attributed to the substitution of hydrogen atom connecting with nitrogen atom replaced by methyl or ethyl group leads to the decreased hydrogen bonding interaction. Similar result was also observed for other type porous polymers, for example, the porous benzimidazole-linked polymers showed a high CO_2 uptake ability of up to 5.3 mmol g^{-1} because the hydrogen atom connecting with nitrogen atom of imidazole ring enhanced the interactions between the pore wall and CO_2 molecules through hydrogen bonding.[29] The CO_2 uptake capacity of 3.30 mmol g^{-1} for TBMID is higher than that of many other reported

CMPs produced by Sonogashira-Hagihara coupling reaction under the same conditions, such as the post-metalation of porous aromatic framework of PAF-26-COOMg (2.85 mmol g^{-1}, S_{BET} = 572 m^2 g^{-1}),[52] the amide-functionalized CMP of CMP-1-AMD1 (1.51 mmol g^{-1}, S_{BET} = 316 m^2 g^{-1}),[47] the pyrene-based porous aromatic frameworks of PAF-20 (1.16 mmol g^{-1}, S_{BET} = 702 m^2 g^{-1}),[53] the hexabenzocoronene-based porous organic polymers of HBC-POP-1 (2.05 mmol g^{-1} S_{BET} = 668 m^2 g^{-1}),[54] and the tri(4-ethynylphenyl)amine-based porous aromatic frameworks of PAF-34 (2.50 mmol g^{-1}, S_{BET} = 953 m^2 g^{-1})[55] at 273 K/1.0 bar. It is also much higher than that of some other type of porous materials with much higher BET surface area under the same conditions, such as PAF-1 (2.1 mmol g^{-1}, S_{BET} = 5460 m^2 g^{-1}),[56] COF-102 (1.56 mmol g^{-1}, S_{BET} = 3620 m^2 g^{-1})[57] and the tetraphenylmethane-based HCPs (1.66 mmol g^{-1}, S_{BET} = 1679 m^2 g^{-1}),[58] although it is still low compared with some reported porous polymers with high carbon dioxide uptake capacity, such as the imine-linked porous polymer network of (6.1 mmol g^{-1} for PPF-1),[28] the fluorinated covalent triazine-based frameworks (5.53 mmol g^{-1} for FCTF-1-600),[59] the carbazolic porous organic frameworks (4.77 mmol g^{-1} for Cz-POF-3),[60] and the benzimidazole-linked polymers (5.3 mmol g^{-1} for BILP-4).[29] It is known that surface area, micropore volume, pore size and polar groups or moieties have large influence on the CO_2 adsorption performance of microporous organic polymers. For example, TBMID with smaller pore size of 0.9 nm, showed higher CO_2 uptake ability of 3.3 mmol g^{-1} than TBMIDM (pore size 1.1 nm) and TBMIDE (pore size 1.0 nm), which could be attributed to the stronger binding affinity between TBMID and CO_2 molecules, as evidenced by the isosteric heat of CO_2 adsorption (Figure 3d). Therefore, one could expect that the CO_2 uptake ability of these isoindigo-based microporous organic polymers could be further improved by

optimizing surface area, pore size or introducing some strong polar groups into the skeleton of the polymers.

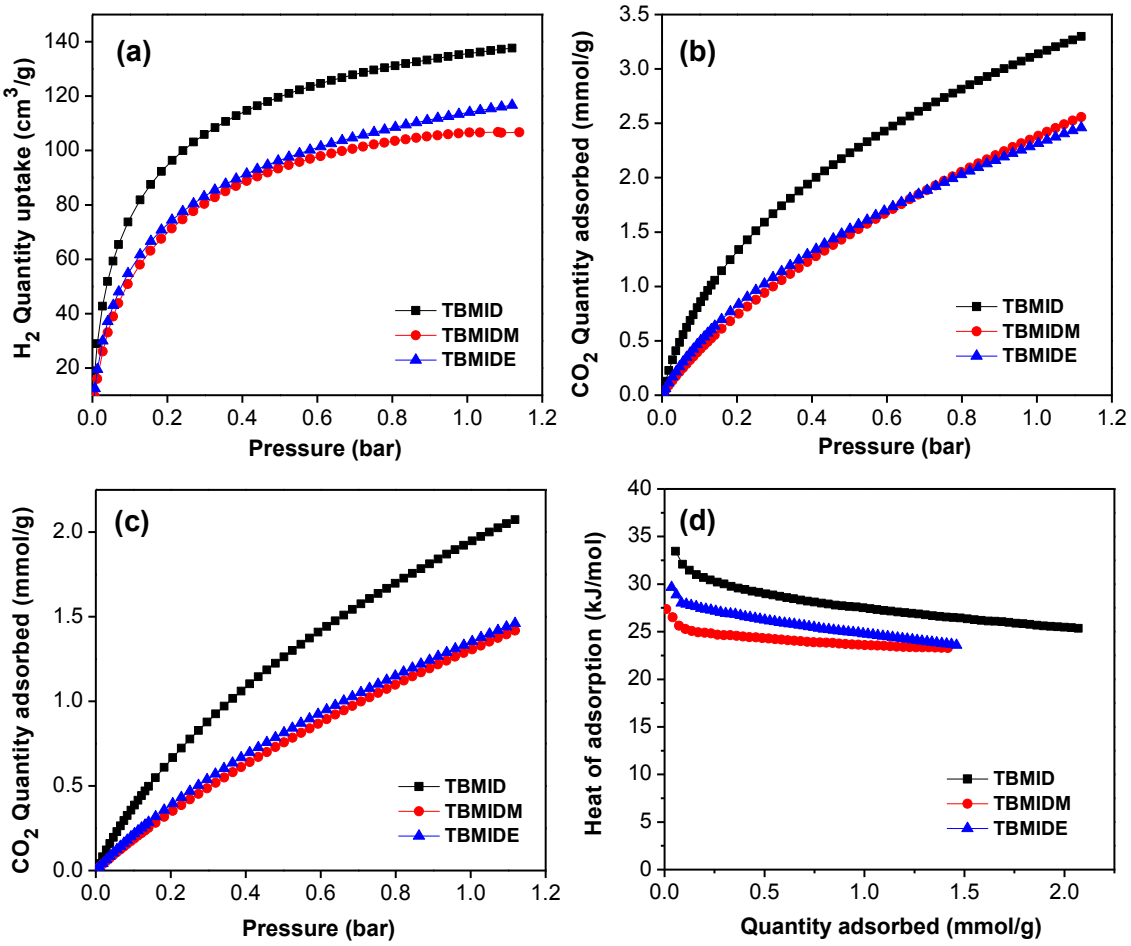

Figure 3. a) Volumetric H_2 sorption curves for the polymer networks at 77.3 K up to 1.13 bar; b) CO_2 adsorption isotherms collected at 273 K ; c) CO_2 adsorption isotherms collected at 298 K; d) Isosteric heats of adsorption for CO_2 calculated from the adsorption isotherms collected at 273 K and 298 K.

The isosteric heat of adsorption (Q_{st}) was calculated from the CO_2 adsorption data collected at 273 K and 298 K by the Clausius–Clapeyron equation to determine the binding affinity between the polymers and CO_2 molecules. As shown in Figure 3d, the Q_{st} values of the polymer networks were found to be in the range of 27.4–33.5 kJ mol^{-1} at the near zero-coverage, which are comparable to those of many known functionalized porous polymers, such as the porous benzimidazole-linked polymers (26.7–28.8 kJ mol^{-1}),[29] the carbazole-based CMPs (27.1–30.8 kJ mol^{-1}),[43] the

tetraphenylethylene-based HCPs (23.3–28.2 kJ mol^{-1}),[61] the metalation of CMPs (PAF-26-COONa, 35 kJ mol^{-1}),[52] the sulfonated porous polymer network (PPN-6-SO_3Li, 35.7 kJ mol^{-1})[62] and the porous polymer network (PPN-6-SO_3NH_4, 40 kJ mol^{-1}).[63] This result demonstrated that the incorporation of isoindigo unit into the skeleton of the porous polymers indeed enhanced the binding affinity between the porous polymer and CO_2 molecules, and thus leading to the increased CO_2 uptake ability. In addition, TBMID showed the highest Q_{st} (33.5 kJ mol^{-1}) among the three polymer networks owing to its smaller micropore size and the strong interactions between the polymer network and the polarizable CO_2 molecules through dipole−quadrupole interactions and/or hydrogen bonding as discussed above. In order to investigate the potential use of these isoindigo-functionalized microporous organic polymers in gas separation, single component gas adsorption isotherms for CO_2, N_2, and CH_4 were measured by volumetric methods at 273 K up to a pressure of 1.0 bar The selectivities of CO_2/N_2 and CO_2/CH_4 for the polymer networks were estimated by using the initial slope ratios from the Henry's law constants of the single-component gas adsorption isotherms collected at 273 K at a low pressure coverage less than 0.1 bar as summarized in Table 2 (Figure S7-9). Compared with TBMIDM and TBMIDE, TBMID showed higher CO_2/N_2 and CO_2/CH_4 adsorption selectivities (Table 2). Though the CO_2/N_2 adsorption selectivity of 58.8 for TBMID is moderate compared with that of some other reported MOPs with higher CO_2/N_2 adsorption selectivity, such as the tetraphenylethylene-based HCPs (119 for Network-7),[61] the azo-bridged covalent organic polymer (109 for Azo–COP-2),[64] the porous covalent electron-rich organonitridic frameworks (109 for PECONF-1),[65] and the tri(4-ethynylphenyl) amine-based porous aromatic framework (251 for PAF-33–NH_2),[55] TBMID showed much higher CO_2 adsorption capacity (Network-7: 1.92 mmol g^{-1},[61] Azo-COP-2: 2.55

mmol g^{-1},[64] PECONF-1: 1.86 mmol g^{-1},[65] and PAF-33-NH_2: 1.19 mmol g^{-1} [55]) under the same conditions. From the practical CO_2 separation application of view, both high CO_2 capture capacity and high selectivity of CO_2 over N_2 and CH_4 are required. Therefore, these isoindigo-based microporous organic polymers would be potential candidates for applications in post-combustion CO_2 capture and sequestration because of their good CO_2 adsorption performances.

Table 2. Summary of gas uptakes for the polymer networks

Polymer	H_2 uptake[a] [wt%]	CH_4 uptake[b] [mmol g^{-1}]	CO_2 uptake[b] [mmol g^{-1}]	CO_2 uptake[c] [mmol g^{-1}]	Selectivity[d]	
					CO_2/N_2	CO_2/CH_4
TBMID	1.23	0.75	3.30	2.07	58.8	9.7
TBMIDM	0.95	0.79	2.56	1.42	29.3	4.5
TBMIDE	1.04	0.86	2.46	1.46	42.6	4.3

[a] Data obtained at 77.3 K and 1.13 bar; [b] Data collected at 273 K and 1.13 bar; [c] Data collected at 298 K and 1.13 bar; [d] Adsorption selectivity based on the Henry's law.

4. Conclusions

In conclusion, isoindigo functionalized microporous organic polymers have been synthesized via palladium-catalyzed Sonogashira-Hagihara cross-coupling reaction of 6,6'-dibromoisoindigo or its alkylated derivatives with tetra(4-ethynylphenyl)-methane. These polymer networks are stable in various solvents tested and thermally stable in nitrogen atmosphere. The alkyl groups have an influence on the pore size and surface area of the resulting microporous organic polymers. Owing to the incorporation of electron-rich isoindigo unit into the skeleton of the porous polymers enhanced the binding affinity between the porous polymer and CO_2 molecules, all of the resulting polymers show high isosteric heats of CO_2 adsorption from 27.4 to 33.5 kJ mol^{-1}. The polymer TBMID without any alkyl substituent shows a high CO_2 uptake ability of 3.30 mmol g^{-1} and a CO_2/N_2 adsorption selectivity of 58.8 because of the

strong interactions between the polymer network and the polarizable CO_2 molecules through dipole−quadrupole interactions and/or hydrogen bonding that utilize the protonated and proton-free nitrogen sites of isoindigo segments. These results indicated that there is a wealth of opportunity for producing CO_2-philic microporous organic polymers with enhanced gas adsorption ability and high adsorption selectivity for CO_2 over N_2 by incorporating electron-rich unit into the skeleton of a MOP.

Electronic Supplementary Information (ESI) available: Details of the synthesis for TBMIDM, TBMIDE and the TGA, FT-IR, PXRD, SEM, HR-TEM images, and gas adsorption for the polymer networks. See DOI:XXX/XXX.

Acknowledgments

This work was supported by the National Natural Science Foundation of China (21304055), Research Fund for the Doctoral Program of Higher Education of China (20120202120007), Shaanxi Innovative Team of Key Science and Technology (2013KCT-17), the Fundamental Research Funds for the Central Universities (GK201501002, GK201101003 & GK201301002), and the Open Fund of the State Key Laboratory of Luminescent Materials and Devices (2015-skllmd-04).

References

1. F. X. Li and L. S. Fan, *Energy Environ. Sci*., 2008, **1**, 248-267.
2. R. V. Siriwardane, M. S. Shen and E. P. Fisher, *Energy Fuels*, 2003, **17**, 571-576.
3. C. Lu, H. Bai, B. Wu, F. S. Su and J. F. Hwang, *Energy Fuels*, 2008, **22**, 3050-3056.
4. K. Sumida, D. L. Rogow, J. A. Mason, T. M. McDonald, E. D. Bloch, Z. R. Herm, T.-H. Bae and J. R. Long, *Chem. Rev*., 2011, **112**, 724-781.
5. T. Tozawa, J. T. Jones, S. I. Swamy, S. Jiang, D. J. Adams, S. Shakespeare, R. Clowes, D. Bradshaw, T. Hasell, S. Y. Chong, C. Tang, S. Thompson, J. Parker, A. Trewin, J. Bacsa, A. M.

Slawin, A. Steiner and A. I. Cooper, *Nat. Mater.*, 2009, **8**, 973-978.

6. Y. Jin, B. A. Voss, A. Jin, H. Long, R. D. Noble and W. Zhang, *J. Am. Chem. Soc*., 2011, **133**, 6650-6658.

7. R. Dawson, A. I. Cooper and D. J. Adams, *Prog. Polym. Sci*., 2012, **37**, 530-563.

8. Z. H. Xiang and D. Cao, *J. Mater. Chem. A*, 2013, **1**, 2691-2718.

9. N. B. McKeown and P. M. Budd, *Macromolecules*, 2010, **43**, 5163-5176.

10. T. C. Drage, C. E. Snape, L. A. Stevens, J. Wood, J. Wang, A. I. Cooper, R. Dawson, X. Guo, C. Satterley and R. Irons, *J. Mater. Chem*., 2012, **22**, 2815-2823.

11. Y. Zhang and S. N. Riduan, *Chem. Soc. Rev*., 2012, **41**, 2083-2094.

12. P. Kaur, J. T. Hupp and S. T. Nguyen, *ACS. Catal*., 2011, **1**, 819-835.

13. X. M. Liu, Y. H. Xu and D. L. Jiang, *J. Am. Chem. Soc*., 2012, **134**, 8738-8741.

14. Z. H. Xiang and D. P. Cao, *Macromol. Rapid Commun*., 2012, **33**, 1184-1190.

15. P. M. Budd, B. S. Ghanem, S. Makhseed, N. B. McKeown, K. J. Msayib and C. E. Tattershall, *Chem. Commun*., 2004, 230-231.

16. A. P. Côté, A. I. Benin, N. W. Ockwig, M. O'Keeffe, A. J. Matzger and O. M. Yaghi, *Science*, 2005, **310**, 1166-1170.

17. S. Y. Ding and W. Wang, *Chem. Soc. Rev*., 2013, **42**, 548-568.

18. J. X. Jiang, F. Su, A. Trewin, C. D. Wood, N. L. Campbell, H. Niu, C. Dickinson, A. Y. Ganin, M. J. Rosseinsky, Y. Z. Khimyak and A. I. Cooper, *Angew. Chem. Int. Ed*., 2007, **46**, 8574-8578.

19. A. I. Cooper, *Adv. Mater*., 2009, **21**, 1291-1295.

20. J. X. Jiang and A. I. Cooper, *Topics. Curr. Chem*., 2010, **293**, 1-33.

21. D. Yuan, W. Lu, D. Zhao and H. C. Zhou, *Adv. Mater*., 2011, **23**, 3723-3725.

22. T. Ben, H. Ren, S. Ma, D. Cao, J. Lan, X. Jing, W. Wang, J. Xu, F. Deng, J. M. Simmons, S. Qiu and G. Zhu, *Angew. Chem. Int. Ed*., 2009, **48**, 9457-9460.

23. P. Kuhn, M. Antonietti and A. Thomas, *Angew. Chem. Int. Ed*., 2008, **47**, 3450-3453.

24. J. Germain, J. Hradil, J. M. Fréchet and F. Svec, *Chem. Mater*., 2006, **18**, 4430-4435.

25. J. Y. Lee, C. D. Wood, D. Bradshaw, M. J. Rosseinsky and A. I. Cooper, *Chem. Commun*., 2006, 2670-2672.

26. S. J. Xu, Y. L. Luo and B. Tan, *Macromol. Rapid Commun*., 2013, **34**, 471-484.

27. Q. Chen, M. Luo, P. Hammershoj, D. Zhou, Y. Han, B. W. Laursen, C. G. Yan and B. H. Han, *J. Am. Chem. Soc*., 2012, **134**, 6084-6087.

28. Y. L. Zhu, H. Long and W. Zhang, *Chem. Mater*., 2013, **25**, 1630-1635.

29. M. G. Rabbani and H. M. El-Kaderi, *Chem. Mater*., 2012, **24**, 1511-1517.

30. P. Arab, M. G. Rabbani, A. K. Sekizkardes, T. İslamoğlu and H. M. El-Kaderi, *Chem. Mater*., 2014, **26**, 1385-1392.

31. X. Zhu, S. M. Mahurin, S. H. An, C. L. Do-Thanh, C. Tian, Y. Li, L. W. Gill, E. W. Hagaman, Z. Bian, J. H. Zhou, J. Hu, H. Liu and S. Dai, *Chem. Commun*., 2014, **50**, 7933-7936.

32. J. Byun, S.-H. Je, H. A. Patel, A. Coskun and C. T. Yavuz, *J. Mater. Chem. A*, 2014, **2**, 12507-12512.

33. A. Modak, M. Nandi, J. Mondal and A. Bhaumik, *Chem. Commun*., 2012, **48**, 248-250.

34. A. Modak, M. Pramanik, S. Inagaki and A. Bhaumik, *J. Mater. Chem. A*, 2014, **2**, 11642-11650.

35. R. Dawson, D. J. Adams and A. I. Cooper, *Chem. Sci*., 2011, **2**, 1173-1177.

36. J. X. Jiang, C. Wang, A. Laybourn, T. Hasell, R. Clowes, Y. Z. Khimyak, J, Xiao, S. J. Higgins, D. J. Adams and A. I. Cooper, *Angew. Chem. Int. Ed*., 2011, **50**, 1072-1075.

37. P. Zhang, Z. Weng, J. Guo and C. Wang, *Chem. Mater*., 2011, **23**, 5243-5249.

38. Y. Xie, T. T. Wang, X. H. Liu, K. Zou and W. Q. Deng, *Nat. Commun*., 2013, **4**, 1960.

39. R. Stalder, J. Mei, K. R. Graham, L. A. Estrada and J. R. Reynolds, *Chem. Mater*., 2013, **26**, 664-678.

40. W. Ying, F. Guo, J. Li, Q. Zhang, W. Wu, H. Tian and J. Hua, *ACS Appl. Mater. Interfaces*, 2012, **4**, 4215-4224.

41. S. W. Yuan, S. Kirklin, B. Dorney, D. J. Liu and L. P. Yu., *Macromolecules*, 2009, **42**, 1554-1559.

42. K. Sing, D. Everett, R. Haul, L. Moscou, R. Pierotti, J. Rouquerol and T. Siemieniewska, *Pure Appl. Chem*., 1985, **57**, 603-619.

43. X. Y. Wang, Y. Zhao, L. L. Wei, C. Zhang, X. Yang, M. Yu and J. X. Jiang, *Macromol. Chem. Phys*., 2015, **216**, 504-510.

44. R. Banerjee, H. Furukawa, D. Britt, C. Knobler, M. O'Keeffe and O. M. Yaghi, *J. Am. Chem. Soc*., 2009, **131**, 3875-3877.

45. B. P. Biswal, S. Chandra, S. Kandambeth, B. Lukose, T. Heine and R. Banerjee, *J. Am. Chem. Soc*., 2013, **135**, 5328-5331.

46. L. M. Lanni, R. W. Tilford, M. Bharathy and J. J. Lavigne, *J. Am. Chem. Soc*., 2011, **133**, 13975-13983.

47. T. Ratvijitvech, R. Dawson, A. Laybourn, Y. Z. Khimyak, D. J. Adams and A. I. Cooper, *Polymer*, 2014, **55**, 321-325.

48. C. Zhang, X. Yang, Y. Zhao, X. Wang, M. Yu and J. X. Jiang, *Polymer*, 2015, **61**, 36-41.

49. R. Dawson, A. Laybourn, R. Clowes, Y. Z. Khimyak, D. J. Adams and A. I. Cooper., *Macromolecules*, 2009, **42**, 8809-8816.

50. J. X. Jiang, F. Su, A. Trewin, C. D. Wood, H. Niu, J. T. Jones, Y. Z. Khimyak and A. I. Cooper, *J. Am. Chem. Soc*., 2008, **130**, 7710-7720.

51. R. M. Kassab, K. T. Jackson, O. M. El-Kadri and H. M. El-Kaderi, *Res. Chem. Intermed*., 2011, **37**, 747-757.

52. H. P. Ma, H. Ren, X. Q. Zou, S. Meng, F. X. Sun and G. S. Zhu, *Polym. Chem*., 2014, **5**, 144-152.

53. Z. J. Yan, H. Ren, H. P. Ma, R. R. Yuan, Y. Yuan, X. Q. Zou, F. X. Sun and G. S. Zhu, *Micropor. Mesopor. Mater*., 2013, **173**, 92-98.

54. C. M. Thompson, F. Li and R. A. Smaldone, *Chem. Commun*., 2014, **50**, 6171-6173.

55. R. R. Yuan, H. Ren, Z. J. Yan, A. Wang and G. S. Zhu, *Polym. Chem*., 2014, **5**, 2266.

56. T. Ben, C. Y. Pei, D. L. Zhang, J. Xu, F. Deng, X. F. Jing and S. L. Qiu, *Energy Environ. Sci*., 2011, **4**, 3991.

57. H. Furukawa and O.M. Yaghi, *J. Am. Chem. Soc*., 2009, **131**, 8875-8883.

58. X. F. Jing, D. L. Zou, P. Cui, H. Ren and G. S. Zhu, *J. Mater. Chem. A*, 2013, **1**, 13926-13931.

59. Y. F. Zhao, K. X. Yao, B. Y. Teng, T. Zhang and Y. Han, *Energy Environ. Sci*., 2013, **6**, 3684-3692.

60. X. Zhang, J. Z. Lu and J. Zhang, *Chem. Mater.*, 2014, **26**, 4023-4029.

61. S. W. Yao, X. Yang, M. Yu, Y. H. Zhang and J. X. Jiang, *J. Mater. Chem. A*, 2014, **2**,

8054-8059.

62. W. Lu, D. Yuan, J. Sculley, D. Zhao, R. Krishna and H. C. Zhou, *J. Am. Chem. Soc*., 2011, **133**, 18126-18129.

63. W. G. Lu, W. M. Verdegaal, J. M. Yu, P. B. Balbuena, H.-K. Jeong and H.-C. Zhou, *Energy Environ. Sci*., 2013, **6**, 3559-3564.

64. H. A. Patel, S. H. Je, J. Park, Y. Jung, A. Coskun and C. T. Yavuz, *Chem.-A Eur. J*., 2014, **20**, 772-780.

65. P. Mohanty, L. D. Kull and K. Landskron, *Nat. Commun*., 2011, **2**, 401.

Table of Contents

Isoindigo-based microporous organic polymers show a high CO_2 uptake ability of 3.30 mmol g^{-1} (1.13 bar/273 K) with a CO_2/N_2 sorption selectivity of 58.8:1.

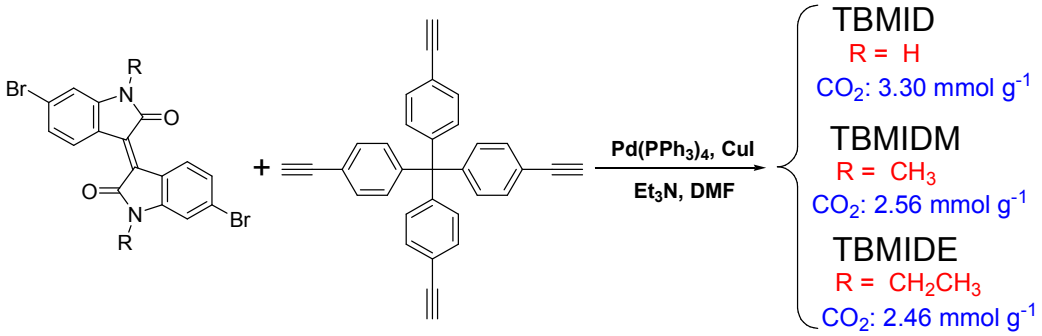

Yang Zhao, Xiaoyan Wang, Chong Zhang, Fangyuan Xie, Rui Kong, Jia-Xing Jiang*

Isoindigo-Based Microporous Organic Polymers for Carbon Dioxide Capture